



Visualization of nuclear many-body correlations with the most probable configuration of nucleonsMoemi Matsumoto ¹ and Yusuke Tanimura ^{1,2}¹*Department of Physics, Tohoku University, Sendai 980-8578, Japan*²*Graduate Program on Physics for the Universe, Tohoku University, Sendai 980-8578, Japan*

(Received 17 April 2022; accepted 1 July 2022; published 13 July 2022)

A method to visualize many-body correlations using the information of the full wave function is presented. The set of nucleon coordinates which maximizes the square of the wave function, that is, the most probable spatial configuration of nucleons, is visualized. The method is applied to Hartree-Fock (HF) and HF+BCS wave functions of p - and sd -shell $N = Z$ even-even nuclei to analyze the many-body correlations in those systems. It is found that there are α -cluster-like four-body correlations already at the HF level in some of the nuclei. The effects of pairing on the most probable configuration are also investigated. The method is useful to analyze the nuclear many-body correlations, and it suggests a new viewpoint to microscopic nuclear wave functions.

DOI: [10.1103/PhysRevC.106.014307](https://doi.org/10.1103/PhysRevC.106.014307)**I. INTRODUCTION**

The nuclear many-body wave function contains an enormous amount of information since it is, for an A -body system, a function of $3A$ continuous variables for positions and $2A$ discrete variables for spins and isospins. Therefore, in general it is difficult to analyze the full information of the wave function. Moreover, many of the experimental observables are expectation values or transition probabilities of one- or two-body operators. For these reasons, theoretical analyses in nuclear physics are made mainly for quantities obtained after integrating out most of the information of correlations embedded in a many-body wave function, such as one- and two-body densities.

A typical example of spatial nucleon correlations is clustering. Cluster model calculations have been successfully applied mainly to light systems where some specific cluster structure is explicitly assumed [1–4]. Studies of the cluster structure based on microscopic theories without assuming any clusters have been made with the one-body density [5–8] and two-body density (the localization function) [9–14] in the coordinate space. There was also an analysis of the overlaps between α -cluster-model and mean-field wave functions [15]. The reduced width amplitude and spectroscopic factor can also be used to quantify the existence probability of clusters [16–19].

In the field of quantum chemistry, on the other hand, methods to visualize the spatial correlation among all electrons in a system have been developed and applied to studies of molecular structures [20–23]. The authors of Ref. [20] have developed a method, which they call “dynamic Voronoi metropolis sampling (DVMS),” to efficiently compute the average electron configuration of the system by partitioning the $3N$ -dimensional space of a many-electron wave function into regions related by the permutation symmetry. It provides a way to find out a “representative snapshot” of all the electrons

in a molecule. The method does not rely on the molecular orbitals, which cannot be defined uniquely for a Slater determinant, and are even less well defined when the wave function is given by a superposition of many Slater determinants. Thus it gives a robust way to analyze the wave functions obtained by any theoretical framework, and it would be interesting to apply such a method to the nuclear structure as well.

In this paper, we employ a simpler method: the most probable spatial arrangement of nucleons, i.e., the set of coordinates $(\mathbf{r}_1\sigma_1\tau_1, \mathbf{r}_2\sigma_2\tau_2, \dots, \mathbf{r}_A\sigma_A\tau_A)$ that maximizes $|\Psi|^2$, is searched for and visualized as the likely snapshot of a nucleus. As the first application of the method, we test it with nuclear many-body wave functions obtained by Hartree-Fock (HF) and HF+BCS theories.

The paper is organized as follows. In Sec. II, the method to find the maximum of $|\Psi|^2$ is introduced. In Sec. III we describe the results for the p - and sd -shell $N = Z$ nuclei. A summary and future outlook are given in Sec. IV. In addition, we give in Appendix B the coordinate-space representation of the BCS-type wave function.

II. METHOD: $|\Psi|^2$ MAXIMIZATION

In this section, we present the method that we call the “ $|\Psi|^2$ -maximization method” for visualization of the many-body correlations. The idea is to plot the most probable configuration of all the nucleons in a nucleus.

We consider a time-even many-body state consisting of N ($=$ even) identical fermions. For simplicity we ignore the isospin degrees of freedom. The function to be maximized is the square of the wave function,

$$\rho^{(N)}(x_1, x_2, \dots, x_N) \equiv |\Psi(x_1, x_2, \dots, x_N)|^2, \quad (1)$$

where $x_i \equiv (\mathbf{r}_i\sigma_i)$ denotes the position and spin variables of the i th particle. The superscript (N) emphasizes that this is the “ N -body density,” which is the probability density of finding

the N particles simultaneously at the given set of coordinates. Notice that $\rho^{(N)}$ is invariant under any permutation of the coordinates. To simplify the problem, we define the density within a limited domain of the parameter space,

$$\rho_{d_s}^{(N)}(\mathbf{r}_1, \mathbf{r}_2, \dots, \mathbf{r}_N) \equiv \rho(\underbrace{\mathbf{r}_1 \uparrow, \dots, \mathbf{r}_{N/2+d_s} \uparrow}_{N/2+d_s \text{ up}}, \underbrace{\mathbf{r}_{N/2+d_s+1} \downarrow, \dots, \mathbf{r}_N \downarrow}_{N/2-d_s \text{ down}}), \quad (2)$$

with the spin variables fixed. The integer parameter d_s denotes half the difference between the numbers of spin ups and downs. For example, $d_s = 0$ gives

$$\rho_0^{(N)}(\mathbf{r}_1, \mathbf{r}_2, \dots, \mathbf{r}_N) \equiv \rho(\underbrace{\mathbf{r}_1 \uparrow, \dots, \mathbf{r}_{N/2} \uparrow}_{N/2 \text{ up}}, \underbrace{\mathbf{r}_{N/2+1} \downarrow, \dots, \mathbf{r}_N \downarrow}_{N/2 \text{ down}}), \quad (3)$$

for which the numbers of spin ups and downs are equal. The function $\rho_{d_s}^{(N)}$ depends only on continuous variables $\mathbf{r}_1, \mathbf{r}_2, \dots, \mathbf{r}_N$. Note again that the order of the spatial coordinates within those with the same spin orientation is irrelevant. Due to the time-reversal invariance of the many-body state, it suffices to consider only $\rho_{d_s \geq 0}^{(N)}$. Thus the task is to maximize $\rho_{d_s}^{(N)}$ for $0 \leq d_s \leq N/2$ and locate the global maximum. Then we plot the set of coordinates, which maximizes $\rho^{(N)}$, in the three-dimensional space, specifying also the spin orientations.

The $|\Psi|^2$ -maximization method gives a qualitative and intuitive picture for the many-body correlations but does not give a quantitative measure for degree of clustering or other types of correlation. The method is still under development towards more extensions and applications, as we will mention in Sec. IV.

Note that, by maximization, one only finds the maximum of the probability distribution and does not pay attention to its global behavior, such as the fluctuation around the maximum or the existence of local maxima. It is also pointed out in Ref. [20] that the maximum of an electronic wave function in a molecule is not always representative, and it may lead to a misleading picture for molecular-bond structure. Therefore, to study the many-body correlations in more detail, it is important to investigate the global behaviors as well as the maximum. Nevertheless, in this paper, we try this simple $|\Psi|^2$ maximization to investigate what we can see from the nuclear many-body wave function.

We should also point out that analyses of the full wave function $|\Psi(x_1, \dots, x_N)|^2$ or its maximum have already been made in few-body calculations [24–27]. There is also a method to determine the “physical coordinates” of nucleons in the antisymmetrized molecular dynamics wave function [28]. The $|\Psi|^2$ maximization presented in this work gives a more general way to perform similar analyses for systems of many particles and for general types of wave functions.

III. RESULTS AND DISCUSSION

We test the $|\Psi|^2$ -maximization method with nuclear wave functions of light $N = Z$ nuclei obtained by microscopic theories.

Due to the short-range and attractive natures of the nucleon-nucleon force, it is reasonable to assume for the nuclear ground states that the maximum of $\rho_{d_s=0}^{(N)}$ is the global maximum of $\rho^{(N)}$. Thus we will show in this section only the maximum of $\rho_0^{(N)}$ for all the systems that we examine (see Appendix A for d_s dependence of the maximum value of $\rho_{d_s}^{(N)}$ for ^{20}Ne nucleus as an example). The neutron-proton formalism is employed in the present framework, and the half of the spins are fixed to be up and the other half down each for neutron and proton sector.

A. Setup

We take Hartree-Fock (HF) and HF+BCS wave functions with the SLy4 Skyrme effective interaction [29] for the HF part and the constant-gap approximation for the BCS part. The HF+BCS state is obtained as usual by adjusting the Fermi energies to get the correct average particle numbers. We impose the axial and reflection symmetries, and the time-reversal symmetry [30]. Note that, in the present calculation, the wave function is given as a product of the neutron and proton parts, each of which depends only on the neutron and proton coordinates, respectively. Therefore, there is no explicit correlation between neutrons and protons, and the maximum search can be carried out separately. The maximum search is performed with the conjugate gradient (CG) method [31] starting from a random initial configuration for the set of spatial coordinates.

One needs values of the wave function $\Psi(x_1, x_2, \dots, x_N)$ for any given set of coordinates. The wave function of a HF state is given by a Slater determinant. The wave function of the N -particle component of a HF+BCS state is given by a Pfaffian. See Appendix B for the explicit expression of the BCS wave function in the coordinate-space representation.

Some remarks on the correlations present in the mean-field wave function are in order. The Pauli principle, of course, is explicitly taken into account by antisymmetrization. There are also the long-range correlations through the mean fields due to the interaction, which roughly determine the nuclear (intrinsic) density distribution [32]. In particular, the deformation induces collective correlations that bring some nucleons to one side and some others to another side of nucleus. In addition, in $N = Z$ nuclei, the neutron and proton wave functions differ only slightly because of the Coulomb force, which is also an implicit but dynamical correlation through the mean fields due to the attraction between neutrons and protons. The deformation and its coherence between neutrons and protons together could lead to cluster correlations in some deformed nuclei, as will be seen later. Furthermore, when the nn and pp pairing correlations are taken into account, one would expect that there will be an additional attractive correlation between spin-up and -down nucleons. The effect of pairing on the correlation between spin-up and -down will also be investigated.

We also remark on the symmetries imposed in the present calculations. Because of the axial symmetry around the z axis, $|\Psi|^2$ is invariant under the simultaneous rotation of all the coordinates around z axis. Furthermore, since the present HF and HF+BCS wave functions are given as a product of neutron and proton parts, $|\Psi|^2$ is independent of the relative angle

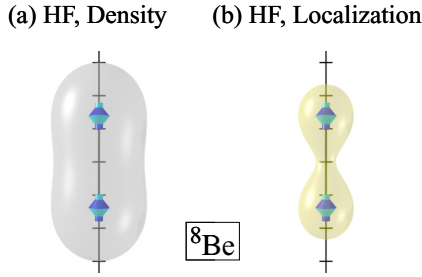


FIG. 1. The most probable configuration of spin-up (-down) neutrons in the HF ground state of ${}^8\text{Be}$ are shown with blue (sky blue) arrows together with (a) the neutron one-body density and (b) the neutron localization function $\bar{C}_{n\uparrow}$. The density isosurface in (a) is drawn at half the maximum value, while the localization function in (b) is drawn at 0.8 times the maximum.

around the z axis between the neutron and proton coordinates. The same applies to the reflection symmetry as well: $|\Psi|^2$ is left unchanged under reflection of all the neutron and/or proton positions and spins.

B. Ground states of s - and sd -shell $N = Z$ nuclei

Now we present the results for the ground states of ${}^8\text{Be}$, ${}^{12}\text{C}$, ${}^{16}\text{O}$, ${}^{20}\text{Ne}$, ${}^{24}\text{Mg}$, and ${}^{28}\text{Si}$ nuclei. Since neutron and proton wave functions are almost the same in $N = Z$ system and there is no explicit correlation between neutrons and protons, we shall show only the most probable configurations of neutrons.

Figures 1–6 show the most probable arrangements of neutrons in the mean-field ground states. The positions of spin-up (-down) neutrons are represented with blue (sky blue) arrows, together with the isosurfaces of the neutron one-body density and localization function [9,33]. The density isosurface is drawn at half the maximum value while the localization function (multiplied by the one-body density), as defined below in Eq. (5), is drawn at 0.8 times the maximum. The bars in the figures connecting the arrows are added to clarify the structures but do not have a physical significance. The vertical axis is the symmetry axis, and the ticks on it are located every 1 fm.

The localization function shown in Figs. 1–6(b) is a measure of localization in the HF wave function, which is related to the spatial two-body correlation between two like-spin fermions of the same kind [9–14,33,34]. It was developed in quantum chemistry [33] and introduced to nuclear physics in Ref. [9]. It was recently used also to study the extra kinetic energy due to the Pauli exclusion during the collision process [35]. The localization function for a particle of kind $q = n$ or p with spin $\sigma = \uparrow$ or \downarrow is defined as

$$C_{q\sigma}(\mathbf{r}) = \left[1 + \left(\frac{\rho_{q\sigma} \tau_{q\sigma} - \mathbf{j}_{q\sigma} - \frac{1}{4} \nabla(\rho_{q\sigma})^2}{\rho_{q\sigma} \tau_{q\sigma}^{\text{TF}}} \right)^2 \right]^{-1}, \quad (4)$$

where $\rho_{q\sigma}$, $\tau_{q\sigma}$, and $\mathbf{j}_{q\sigma}$ are the one-body density, kinetic-energy density, and current density of particle $q\sigma$, respectively, and $\tau_{q\sigma}^{\text{TF}} = \frac{3}{5} (6\pi)^{2/3} \rho_{q\sigma}^{5/3}$ is the Thomas-Fermi kinetic-energy density. A value of $C_{q\sigma}$ close to 1 implies the

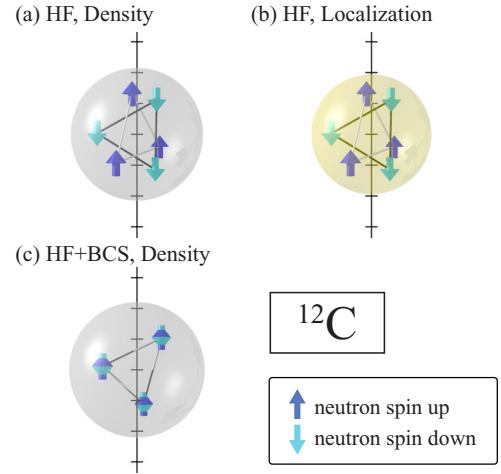


FIG. 2. The most probable configurations of spin-up (-down) neutrons obtained by the HF and the HF+BCS wave functions in the ground state of ${}^{12}\text{C}$ nucleus are shown with blue (sky blue) arrows. We show (a) the HF result together with the neutron one-body density, (b) the HF result together with the neutron localization function, and (c) the HF+BCS result together with the neutron one-body density. The density isosurface is drawn at half the maximum value, while the localization function is drawn at 0.8 times the maximum. See the Supplemental Material [36] for the animated views of (a) and (c).

signature of localization, which means that the probability of finding two particles of $q\sigma$ close to each other is very low. $C_{q\sigma} \approx 1$ simultaneously for all the spin-isospin combinations is a minimal necessary condition of α clusterization [9]. In the present case with $N = Z$ and time-reversal symmetry, the wave functions of neutron and proton are approximately the same, and $C_{q\uparrow}$ and $C_{q\downarrow}$ are exactly the same, so it suffices to consider only $C_{n\uparrow}$. Since the localization is not a meaningful quantity in the regions where the one-body density is close to zero, we look at the localization function multiplied by the

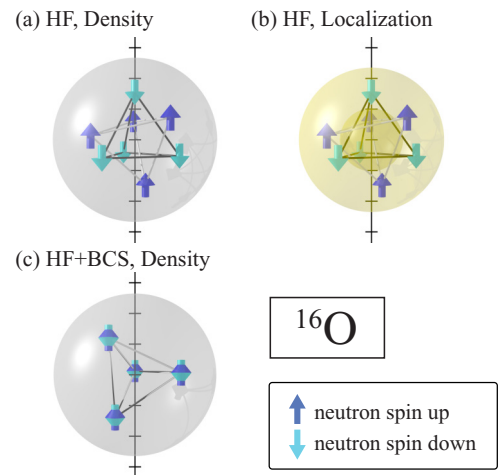


FIG. 3. The same as Fig. 2 but for the ground state of ${}^{16}\text{O}$ nucleus. There are two surfaces for the localization function because it is peaked around 1.5 fm away from the center of the nucleus.

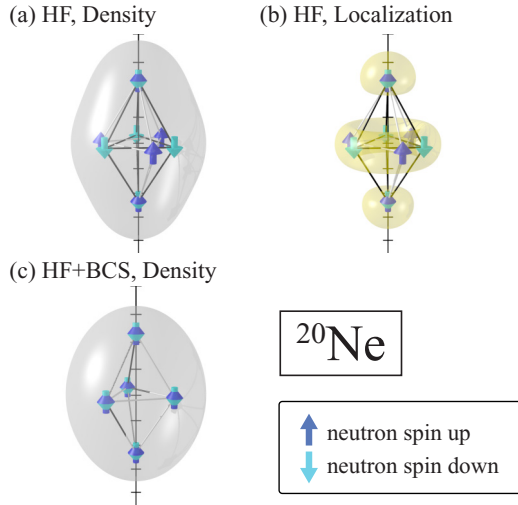


FIG. 4. The same as Fig. 2 but for the ground state of the ^{20}Ne nucleus.

normalized one-body density,

$$\bar{C}_{q\sigma}(\mathbf{r}) = C_{q\sigma}(\mathbf{r}) \frac{\rho_{q\sigma}(\mathbf{r})}{\max \rho_{q\sigma}(\mathbf{r})}, \quad (5)$$

as was done in Ref. [10].

The localization function is shown for comparison with the result of $|\Psi|^2$ maximization. Notice that the localization function only represents the two-body correlation between nucleons with the same spin and tells nothing about the correlation between different spins. On the other hand, one can see the correlations between spin-up and -down neutrons as well with the $|\Psi|^2$ -maximization method since it is based on the full information the wave function and takes into account the correlations among all nucleons.

Figure 1 shows the result for the HF ground state of ^8Be nucleus. It is well established that the nucleus has very pronounced 2α structure, and its mean-field wave function indeed exhibits such structure. One sees that pairs of spin-up and

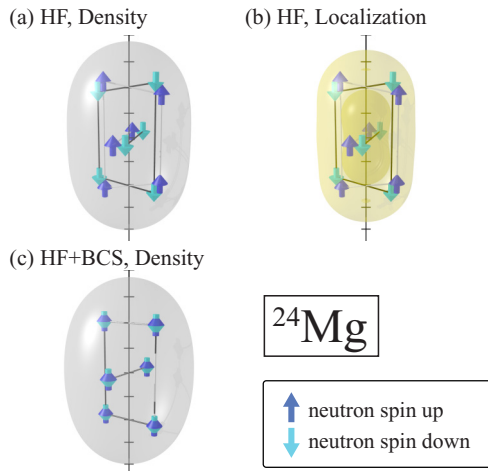


FIG. 5. The same as Fig. 2 but for the ground state of the ^{24}Mg nucleus.

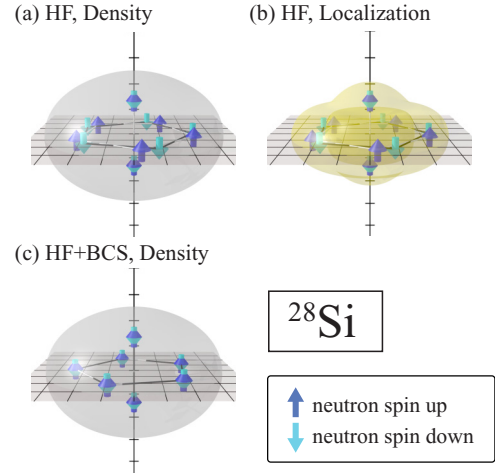


FIG. 6. The same as Fig. 2 but for the ground state of the ^{28}Si nucleus.

-down neutrons are located at the upper and lower part of the system. Since the proton configuration is almost identical to that of neutrons, there are quartets of nucleons consisting of different spins and isospins at almost the same position. It indicates that there are two α -cluster-like objects in this system. The neutron localization function, which may be regarded as a measure of α clustering, shown in Fig. 1(b), has large values around the most probable positions of the neutrons. Thus one finds that the implication about α clustering of the localization function is consistent with the picture obtained with the present approach in this particular case.

Figure 2 shows the result for the ^{12}C nucleus. The ^{12}C nucleus is spherical in the present calculations. As seen in Figs. 2(a) and 2(b) for the HF case, the most probable positions of the three neutrons with the same spin form an equilateral triangle. We have found that, in the HF case, there is almost no correlation in the relative angle about z axis between the two triangles. With the pairing correlation, the two triangles are overlaid in the most probable arrangement, as seen in Fig. 2(c) for the HF+BCS case. Thus it turns out, as could be expected, that the pairing correlation induces an attractive correlation between spin-up and -down nucleons. We recall that the protons are not explicitly correlated with the neutrons. Thus, in the present HF and HF+BCS wave functions there are no α -like correlations as observed in the ^8Be case. In the present calculation, only if there is a pair of neutrons on the symmetry axis and $N = Z$ can one say that there is an α -cluster-like four-body correlation.

In ^{16}O nucleus shown in Fig. 3, the four neutrons with the same spin form a regular tetrahedron [Figs. 3(a) and 3(b)]. As in the case of the ^{12}C nucleus, only with the pairing correlation do the spin-up and -down tetrahedrons favor the same orientation. Again, since the protons are not correlated with the neutrons, one cannot claim α -cluster correlation in our present framework. Note that we forced the pairing gaps to be nonzero by the constant-gap approximation although the pairing is not likely to be active in this nucleus.

Figure 4 shows the result for the ^{20}Ne nucleus. In contrast to the two spherical nuclei ^{12}C and ^{16}O , ^{20}Ne is deformed,

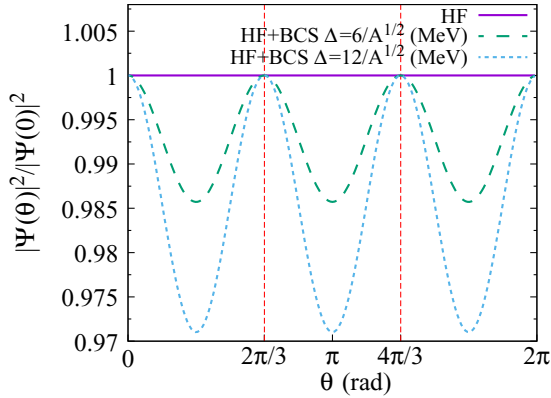


FIG. 7. $|\Psi|^2$ of ^{20}Ne as functions of the relative angle θ between spin-up and -down neutrons. The angle θ is defined as the rotation angle of the positions of spin-up neutrons about the z axis while those of spin-down neutrons are fixed. $\theta = 0$ corresponds to the most probable configuration shown in Fig. 4. The probabilities are normalized with their own maximum values. The solid curve represents the HF result, and the dashed and dotted curves show the HF+BCS results with pairing gaps $\Delta = 6/A^{1/2}$ MeV and $\Delta = 12/A^{1/2}$ MeV, respectively.

and interesting cluster structure associated with it is observed with our method. As seen in Fig. 4, there are two α clusters at the top and bottom along the z axis, and at the middle are two regular triangles of spin-up and -down neutrons, respectively. As can be seen in Fig. 4(b), the nucleons are most likely to be located at the regions where the localization function has large values. However, despite the large values of the localization function at the middle of the system, we conclude from our analysis that α particles are not likely to exist around there in the present mean-field wave functions. As we shall see later, without pairing, there is no rotational correlation around the z axis between the spin-up and -down triangles. Moreover, by construction there is no such correlation between neutron and proton triangles as mentioned in the previous subsection. We can only state that in the present setup that each triplet of nucleons with the same spin is likely to form a regular triangle and that 12 nucleons are likely to be located along the circle on the xy plane. With pairing, spin-up and -down triangles of the same nucleon kind favor the same orientation (see Fig. 7). If we took into account explicit neutron-proton correlations via, e.g., neutron-proton pairing or HF quasiparticles with isospin mixing [37–40] in addition to the pairing between like nucleons, there might be α clusters in the middle region as well as the top and bottom. We also note that the “bipyramidal” structure seen in our results supports the assumption of the cluster model employed in Ref. [41], if one is concerned only with neutrons or protons.

Figure 5 shows the results for the ^{24}Mg nucleus. In the HF case [Fig. 5(a)], four of the spin-up neutrons form a trapezoid, while the remaining two are located at both sides of it. The spin-down neutrons are arranged symmetrically with the spin-up ones. As a result, there are six close pairs of neutrons. As seen from Fig. 5(b) the neutrons are located in the region where the localization function is larger. With pairing [Fig. 5(c)], the two trapezoids become rectangles,

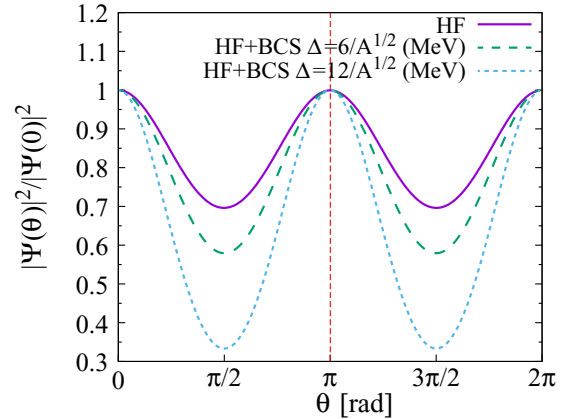


FIG. 8. The same as Fig. 7 but for the ground state of the ^{24}Mg nucleus.

and the arrangements of spin-up and -down nucleons become identical.

Figure 6 shows the results for the ^{28}Si nucleus, which is oblatelly deformed. It is likely that there are two α clusters along the z axis, and regular pentagons are formed on the xy plane by the remaining nucleons with the same spin. The two pentagons coincide with each other with pairing correlations.

Next, we investigate the effects of the pairing correlation by observing the behavior of the probability distribution around the maximum. We pick ^{20}Ne and ^{24}Mg , and we rotate only the positions of spin-up neutrons by angle θ about the z axis while spin-down neutrons are fixed. Figures 7 and 8 show comparisons of the θ dependence of $|\Psi|^2$ with and without the pairing in ^{20}Ne and ^{24}Mg , respectively. The solid curve shows the probability relative to the maximum in the HF case, while the dashed and dotted curves show the same thing with different values of the pairing gap, $\Delta = 6/A^{1/2}$ MeV and $\Delta = 12/A^{1/2}$ MeV, respectively. Since the most probable neutron configuration of the ^{20}Ne (^{24}Mg) nucleus is symmetric under rotation by $2\pi/3$ (π), $|\Psi|^2$ changes periodically. As can be seen in the two figures, as the pairing strength increases, the probability variation also increases. We have also tried a similar analysis on the spherical ^{12}C nucleus by rotating the spin-up neutrons around the z axis while the spin-down neutrons are fixed. We have observed, without pairing, that the probability is nearly constant whereas with pairing the probability changes by $\approx 60\%$.

To briefly summarize the above results, we saw α -like four-body correlations, which are induced by collective deformations and their coherence between neutrons and protons, along the z axis in some of the deformed nuclei. It is also found that the pairing correlation always reinforces the attractive correlations between spin-up and -down nucleons. It is remarkable that the correlation induced by the deformation is reflected in the most likely configuration of nucleons as the cluster-like correlation.

C. Deformed states of ^{16}O

Here we investigate the deformed states of ^{16}O nucleus obtained with constrained HF+BCS calculations. In Fig. 9 we

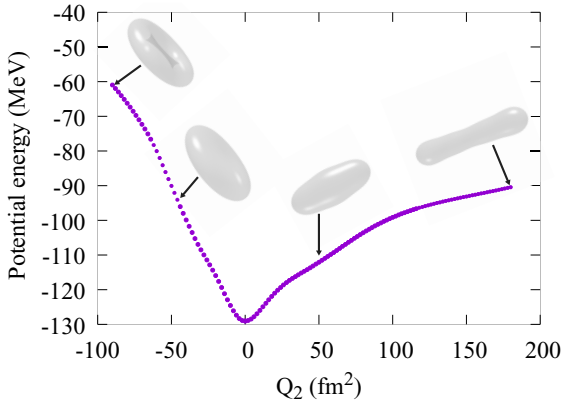


FIG. 9. The HF+BCS potential-energy curve of the ^{16}O nucleus as a function of the quadrupole moment Q_2 . The HF + BCS result is obtained with the constant-gap approximation with the gap parameter $\Delta = 12/A^{1/2}$ MeV. The density isosurfaces at $Q_2 = -90, -50, 50,$ and 180 fm^2 are also shown.

show the potential-energy curve of the nucleus as a function of the quadrupole deformation Q_2 defined as

$$Q_2 = \int d^3r r^2 Y_{20}(\hat{r}) \rho(\mathbf{r}), \quad (6)$$

where $\rho(\mathbf{r})$ is the total one-body density. The ground state is spherical, and, as the deformation increases in the prolate direction, there appears an elongated shape with a bulge at the middle and eventually a rod shape, while at large oblate deformations there appears a torus shape.

We performed the $|\Psi|^2$ maximization for the ^{16}O nucleus with different Q_2 values. The resulting most probable neutron configurations for four selected values of Q_2 are shown in Fig. 10 together with the neutron single-particle energies near the Fermi energies as functions of Q_2 . It is found that there are four regimes of the nucleon arrangement depending on the occupied single-particle levels. We have observed abrupt transitions of the neutron arrangement around the Q_2 values where an alternation of the Fermi level occurs: $Q_2 \approx -25 \text{ fm}^2, 25 \text{ fm}^2,$ and 100 fm^2 (see Supplemental Material [36]). In the most oblate region where $Q_2 \lesssim -25 \text{ fm}^2$, the four pairs of neutrons are most likely to form a square on the xy plane [Fig. 10(a)]. In the near-spherical region, the pairs form a tetrahedron [Fig. 10(b)]. In the prolate region where $25 \lesssim Q_2 \lesssim 100 \text{ fm}^2$, the pairs form a diamond shape aligned to z axis, indicating there are α clusters at the top and the bottom [Fig. 10(c)]. Finally, in the most prolate region ($Q_2 \gtrsim 100 \text{ fm}^2$), all the pairs are located on the z axis, forming a four- α linear chain.

From the various structures obtained by the $|\Psi|^2$ maximization, we found the characteristic arrangements of nucleons in different regimes of deformation or occupied orbitals, which was not clear if we merely observed the shapes.

IV. SUMMARY AND FUTURE PERSPECTIVES

In this paper, we have introduced a method to visualize the many-body correlations based on the full information of the wave function, and demonstrated the usefulness of the method

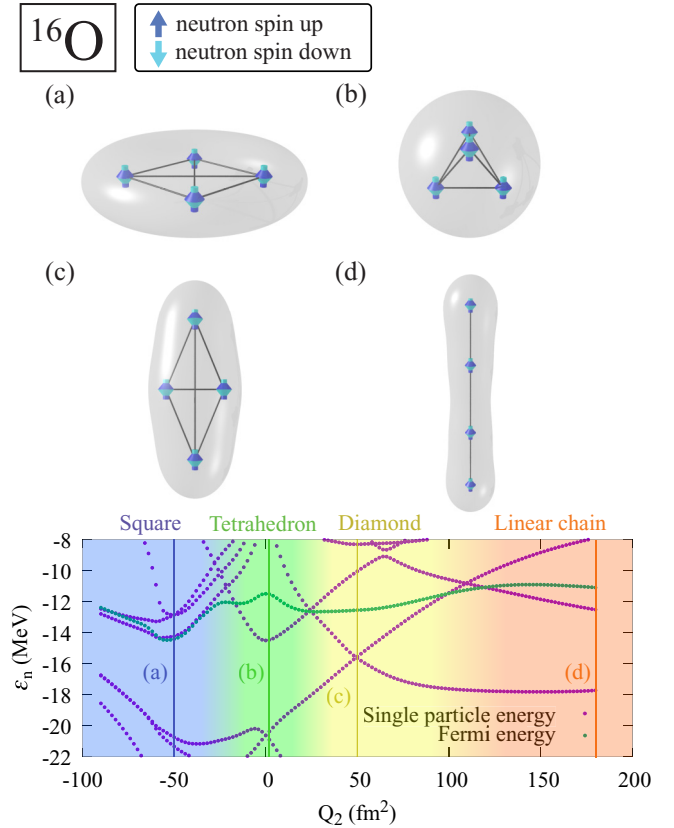


FIG. 10. The most probable neutron configurations of the ^{16}O nucleus at (a) $Q_2 = 50 \text{ fm}^2$, (b) 2 fm^2 , (c) 50 fm^2 , and (d) 180 fm^2 . The lower panel shows the neutron single-particle energies and the Fermi energy as functions of Q_2 . The background colors are inserted according to the four regimes of neutron configurations: square for $Q_2 \lesssim -25 \text{ fm}^2$, tetrahedron for $-25 \text{ fm}^2 \lesssim Q_2 \lesssim 25 \text{ fm}^2$, diamond for $25 \text{ fm}^2 \lesssim Q_2 \lesssim 100 \text{ fm}^2$, and linear chain for $100 \text{ fm}^2 \lesssim Q_2$. The vertical lines labeled by (a)–(d) correspond to the Q_2 values at which the upper figures are obtained. See the Supplemental Material [36] for an animation showing the evolution of the neutron configuration as Q_2 increases.

in nuclear physics. The method visualizes the set of nucleon coordinates which maximizes the square of the many-body wave function. We have applied it to HF and HF+BCS wave functions of p - and sd -shell $N = Z$ even-even nuclei to study the cluster and other correlations in these systems. It was found that the HF wave function already contains α -cluster-like correlations in some deformed nuclei. From the HF+BCS wave functions we found that the pairing correlations induce attractive correlations between spin-up and -down nucleons.

We believe that the present method gives a new viewpoint to the microscopic nuclear wave function. There are several directions for further developments of such methods.

(1) Analyses of more global behaviors of the wave function. In the present work, we only searched for the maximum of $|\Psi|^2$, but it would be necessary and interesting to study more global behaviors as was mentioned in Sec. II. The Markov-chain Monte-Carlo method would be useful to

analyze complicated structures, such as fluctuations and local maxima, of the probability distribution in the multidimensional space.

(2) Applications to more correlated many-body states. The merit of our method is fully exploited when it is applied to a “black box” wave function that contains rich and nontrivial correlations. Thus the shell model or *ab initio* wave functions, which take into account correlations indiscriminately, are more suited for the method. It would also be interesting to analyze the structure of the random-phase approximation or generator-coordinate method wave functions that take into account the correlations associated with collective motions [32,42]. The collective motion would induce fluctuations of the collective degrees of freedom including the cluster structure.

(3) Studies of phenomena other than clustering. There are several phenomena that can be analyzed with the present method or its extensions. The molecular-bond structure accompanying clusters and the correlations among valence neutrons in neutron-rich nuclei can be interesting targets of our analyses. Visualization of motions of individual nucleons during reaction dynamics would also help understanding of mechanisms of fusion, fission, and multinucleon transfer reactions.

ACKNOWLEDGMENTS

The authors are thankful for discussions with Yu Liu, one of the authors of Refs. [20–23]. This work was supported by the JSPS KAKENHI Grant No. 19K03861. M.M. acknowledges support from Graduate Program on Physics for the Universe (GP-PU) of Tohoku University.

APPENDIX A: d_s DEPENDENCE OF $\rho_{d_s}^{(N)}$

In this Appendix, we demonstrate numerically the validity of the assumption made in Sec. III that the maximum of $\rho_{d_s=0}^{(N)}(\mathbf{r}_1, \dots, \mathbf{r}_N)$ [Eq. (2)] is the global maximum of $\rho^{(N)}(x_1, \dots, x_N)$ [Eq. (1)], taking ^{20}Ne as an example.

In Fig. 11, we show the values of $\rho_{d_s}^{(N)}$ with $0 \leq d_s \leq 4$ as functions of CG iterations for the neutron part of the HF wave function of ^{20}Ne nucleus. Although the initial values and the convergence behaviors are different, $\rho_{d_s=0}^{(N)}$ converges indeed to the largest value, and the others converge to values smaller by orders of magnitude. It can also be seen that the maximum values of $\rho_{d_s}^{(N)}$ decrease with the absolute value of d_s .

This example shows the validity of the assumption: it is most likely that the numbers of spin-up and -down nucleons are equal in the ground state so that the nucleons gain energy from the short-range and attractive nucleon-nucleon interaction.

APPENDIX B: BCS WAVE FUNCTION IN COORDINATE-SPACE REPRESENTATION

In this Appendix, we give the expression of the N -particle component of a BCS wave function in the coordinate-space representation, written in terms of the Pfaffian of a certain

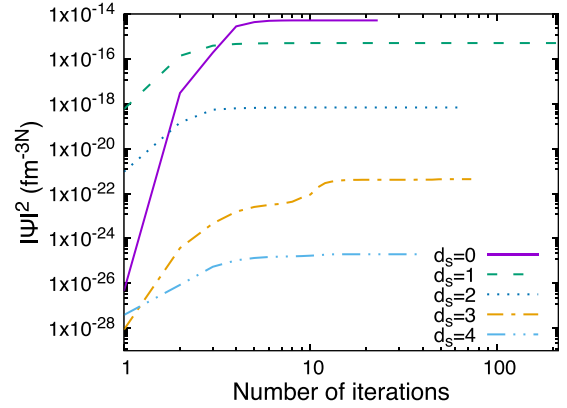


FIG. 11. Values of $\rho_{d_s}^{(N)}$ for $d_s = 0, \dots, 4$ as functions of CG iterations for the neutron part of the wave function of the ^{20}Ne nucleus. The initial spatial neutron coordinates are generated randomly.

matrix. Although the coordinate-space BCS or so-called APG (antisymmetrized product of geminals) wave functions have been discussed and utilized in the context of condensed-matter physics and chemistry [43–46], the notations and structures of their wave functions are suited to many-electron systems rather than nuclear systems. Here we present similar formulas that conform to the nuclear-physics notation. It is remarkable that the formula [Eq. (B24)], given in the form of a Pfaffian, represents the natural generalization of the Slater determinant for HF to the generalized product wave function for BCS or Hartree-Fock-Bogoliubov (HFB) theory [32], including the HF Slater determinant as a special case. We start with a simpler case where all the fermions are paired, then we handle a more complicated situation where there are unpaired particles as well as pairs.

1. Fully paired state

We consider the usual BCS state expressed as

$$|\Psi\rangle = \prod_{k>0} (u_k + v_k a_k^\dagger a_{\bar{k}}^\dagger) |0\rangle \propto \exp\left(\sum_{k>0} \frac{v_k}{u_k} a_k^\dagger a_{\bar{k}}^\dagger\right) |0\rangle, \quad (\text{B1})$$

where $k > 0$ labels a single-particle state, $\bar{k} \equiv -k$ denotes the “conjugate” state to be paired with k [32], and $|0\rangle$ is the bare vacuum. The coefficients u_k and v_k are, in general,

TABLE I. Subsequences $K \in \binom{[N]}{N-M}$, and corresponding K^c and $\text{sgn}(K)$ for $N = 4$ and $M = 2$.

| K | K^c | $\text{sgn}(K)$ |
|-------|-------|-----------------|
| (1,2) | (3,4) | +1 |
| (1,3) | (2,4) | -1 |
| (1,4) | (2,3) | +1 |
| (2,3) | (1,4) | +1 |
| (2,4) | (1,3) | -1 |
| (3,4) | (1,2) | +1 |

complex variational parameters. The exponent of Eq. (B1) can be rewritten as

$$\begin{aligned} \sum_{k>0} \frac{v_k}{u_k} a_k^\dagger a_k^\dagger &= \int dx dx' \sum_{k>0} \frac{v_k}{u_k} \varphi_k(x) \varphi_{\bar{k}}(x') \psi^\dagger(x) \psi^\dagger(x') \\ &= \int dx dx' Z(x, x') \psi^\dagger(x) \psi^\dagger(x'), \end{aligned} \quad (\text{B2})$$

where $\varphi_k(x)$ is the single-particle wave function, $\psi(x)$ is the nucleon field operator, and

$$Z(x, x') \equiv \sum_{k>0} \frac{v_k}{u_k} \varphi_k(x) \varphi_{\bar{k}}(x'). \quad (\text{B3})$$

Note that x denotes the position and the spin variables.

The N -particle component $|\Psi_N\rangle$, where N is even, of the BCS state as given in Eq. (B1) is given up to an unimportant factor by

$$\begin{aligned} |\Psi_N\rangle &\propto \left(\sum_{k>0} \frac{v_k}{u_k} a_k^\dagger a_k^\dagger \right)^{N/2} |0\rangle \\ &= \left(\int dx dx' Z(x, x') \psi^\dagger(x) \psi^\dagger(x') \right)^{N/2} |0\rangle \\ &= \int dx_1 dx_2 \cdots dx_{N-1} dx_N Z(x_1, x_2) \cdots \\ &\quad \times Z(x_{N-1}, x_N) \psi^\dagger(x_1) \psi^\dagger(x_2) \cdots \psi^\dagger(x_{N-1}) \psi^\dagger(x_N) |0\rangle. \end{aligned} \quad (\text{B4})$$

It can then be shown by using the anticommutation relation of the fermion operators that the coordinate-space wave function is given by

$$\begin{aligned} \langle x_1, \dots, x_N | \Psi \rangle &= \langle 0 | \psi(x_1) \cdots \psi(x_N) | \Psi_N \rangle \\ &\propto \sum_{\sigma \in S_N} \text{sgn}(\sigma) Z(x_{\sigma(1)}, x_{\sigma(2)}) Z(x_{\sigma(3)}, x_{\sigma(4)}) \\ &\quad \times \cdots Z(x_{\sigma(N-1)}, x_{\sigma(N)}), \end{aligned} \quad (\text{B5})$$

where S_N is the symmetric group on N objects, and $\text{sgn}(\sigma)$ equals $+1$ (-1) for even (odd) permutations. The above expression can be rewritten as

$$\begin{aligned} \langle x_1, \dots, x_N | \Psi \rangle &\propto \frac{1}{(N/2)!} \sum_{\sigma \in S'_N} \text{sgn}(\sigma) \bar{Z}(x_{\sigma(1)}, x_{\sigma(2)}) \\ &\quad \times \bar{Z}(x_{\sigma(3)}, x_{\sigma(4)}) \cdots \bar{Z}(x_{\sigma(N-1)}, x_{\sigma(N)}), \end{aligned} \quad (\text{B6})$$

where

$$\bar{Z}(x, y) \equiv Z(x, y) - Z(y, x) \quad (\text{B7})$$

and

$$S'_{2n} = \{\sigma \in S_{2n} | \sigma(2i-1) < \sigma(2i) \ (1 \leq i \leq n)\}. \quad (\text{B8})$$

The right-hand side of Eq. (B6) is nothing but the Pfaffian of the following skew symmetric $N \times N$ matrix [47]:

$$\mathcal{Z} = \begin{pmatrix} 0 & \bar{Z}_{12} & \cdots & \bar{Z}_{1N} \\ \bar{Z}_{21} & 0 & \cdots & \bar{Z}_{2N} \\ \vdots & \vdots & \ddots & \vdots \\ \bar{Z}_{N1} & \bar{Z}_{N2} & \cdots & 0 \end{pmatrix}, \quad (\text{B9})$$

where $\bar{Z}_{ij} \equiv \bar{Z}(x_i, x_j) = -\bar{Z}_{ji}$. Therefore, the BCS wave function is given by a Pfaffian,

$$\Psi(x_1, \dots, x_N) \propto \text{pf} \mathcal{Z}. \quad (\text{B10})$$

Due to the property of a Pfaffian that $(\text{pf} A)^2 = \det A$,

$$\rho^{(N)}(x_1, \dots, x_N) = |\Psi(x_1, \dots, x_N)|^2 \propto |\text{pf} \mathcal{Z}|^2 = |\det \mathcal{Z}|. \quad (\text{B11})$$

2. State with unpaired particles

In practical calculations for nuclear systems, the levels far below the fermi level are unpaired and fully occupied, and the v/u factors for these levels tend to diverge. Moreover, for odd nuclei, the last nucleon remains unpaired and blocks a level from the pairing correlation. In such cases, Eq. (B10) is not applicable anymore. Thus now we consider a more general case where $M < N$ single-particles states are unpaired and fully occupied. Such a state is given by

$$|\Psi\rangle = \prod_{i=1}^M a_i^\dagger \prod_{j \geq M+1} (u_j + v_j a_j^\dagger a_j^\dagger) |0\rangle. \quad (\text{B12})$$

If M is an odd number, N is also odd, and $N - M$ is still even. In the same way as the preceding discussion, one obtains, for the coordinate-space representation of the state as given in Eq. (B12),

$$\begin{aligned} \langle x_1, \dots, x_N | \Psi \rangle &\propto \sum_{\sigma \in S_N} \text{sgn}(\sigma) \varphi_1(x_{\sigma(1)}) \cdots \varphi_M(x_{\sigma(M)}) \\ &\quad \times Z(x_{\sigma(M+1)}, x_{\sigma(M+2)}) \cdots \\ &\quad \times Z(x_{\sigma(N-1)}, x_{\sigma(N)}). \end{aligned} \quad (\text{B13})$$

Note that the summation in the function Z [Eq. (B3)] in this case is taken over the levels other than the M fully occupied or blocked ones. Since the number of terms in the summation grows factorially with the number of particles, it is difficult to make a brute-force computation for many-particle systems. We shall show in the following that the right hand side of Eq. (B13) is proportional to a single Pfaffian of an $(N + M) \times (N + M)$ matrix, which is determined by the φ 's and Z 's. Thus $|\Psi|^2$ is easily obtained by computing a determinant.

We will rewrite the right-hand side of Eq. (B13) as a sum of products of a determinant and a Pfaffian. To this end, we first introduce a notation to specify a submatrix of a matrix. Consider an $m \times n$ matrix $X = (x_{ij})_{1 \leq i \leq m, 1 \leq j \leq n}$. Given a subset of r ($\leq m$) row indices $I = \{i_1, i_2, \dots, i_r\}$ and a subset of s ($\leq n$) column indices $J = \{j_1, j_2, \dots, j_s\}$, we denote the $r \times s$ submatrix of X by

$$X(I; J) = (x_{i_p j_q})_{1 \leq p \leq r, 1 \leq q \leq s}. \quad (\text{B14})$$

Next, we define a notation for a subsequence of a sequence of integers. Let $[N]$ be the sequence of positive integers up to N , $\{1, 2, \dots, N\}$. The set of the subsequences of length r of $[N]$

is denoted by $\binom{[N]}{r}$. That is, $\binom{[N]}{r}$ contains all the sequences $\{k_1, k_2, \dots, k_r\}$ such that $1 \leq k_1 < k_2 < \dots \leq N$. Thus each element $K \in \binom{[N]}{r}$ specifies a certain partition of $[N]$ into r numbers and $N - r$ numbers. The complementary sequence of K in $[N]$ is denoted by K^c , which is also arranged in the ascending order.

Let B be an $N \times M$ matrix defined as

$$B = \begin{pmatrix} \varphi_1(1) & \cdots & \varphi_M(1) \\ \varphi_1(2) & \cdots & \varphi_M(2) \\ \vdots & & \vdots \\ \varphi_1(N) & \cdots & \varphi_M(N) \end{pmatrix}, \quad (\text{B15})$$

where $\varphi_i(j) \equiv \varphi_i(x_j)$. Using the notations defined above, one has

$$\begin{aligned} & \sum_{\sigma \in \mathcal{S}_N} \text{sgn}(\sigma) \varphi_1(x_{\sigma(1)}) \cdots \varphi_M(x_{\sigma(M)}) Z(x_{\sigma(M+1)}, x_{\sigma(M+2)}) \cdots \\ & \times Z(x_{\sigma(N-1)}, x_{\sigma(N)}) = \sum_{K \in \binom{[N]}{N-M}} \text{sgn}(K) \\ & \times \text{pf} \mathcal{Z}(K; K) \det B(K^c; [M]), \end{aligned} \quad (\text{B16})$$

where $\text{sgn}(K)$ is the sign of the permutation $\{k_1, \dots, k_{N-M}, k_1^c, \dots, k_M^c\}$ given by concatenating K and

K^c . See Table I for the list of all the possible sequences $K \in \binom{[N]}{N-M}$, and corresponding K^c and $\text{sgn}(K)$ for a simple case where $N = 4$ and $M = 2$. In Eq. (B16), $\text{pf} \mathcal{Z}(K; K)$ is the Pfaffian of an $(N - M) \times (N - M)$ submatrix of \mathcal{Z} while $\det B(K^c; [M])$ is the determinant of an $M \times M$ submatrix of B . Hereafter, we keep K for an element of $\binom{[N]}{N-M}$.

Now we define the following $N \times (N + M)$ matrix:

$$T = (\mathbb{1}_N, B) = \begin{pmatrix} 1 & & & \varphi_1(1) & \cdots & \varphi_M(1) \\ & 1 & & \varphi_1(2) & \cdots & \varphi_M(2) \\ & & \ddots & \vdots & & \vdots \\ & & & 1 & \varphi_1(N) & \cdots & \varphi_M(N) \end{pmatrix}, \quad (\text{B17})$$

where $\mathbb{1}_N$ is the $N \times N$ identity matrix. The submatrix $T([N]; K \cup \{N + 1, \dots, N + M\})$ represents an $N \times N$ matrix,

$$T([N]; K \cup \{N + 1, \dots, N + M\}) = (I'(K), B), \quad (\text{B18})$$

where $I'(K)$ is an $N \times (N - M)$ matrix such that $I'(K)_{kk} = 1$ for $k \in K$ and $= 0$ otherwise. Note that $T([N]; K \cup \{N + 1, \dots, N + M\})$ is given simply by removing the M columns from the $\mathbb{1}_N$ block of T . The determinant of $T([N]; K \cup \{N + 1, \dots, N + M\})$ is given by

$$\begin{aligned} \det T([N]; K \cup \{N + 1, \dots, N + M\}) &= \text{sgn}(K) \det \begin{pmatrix} 1 & & & \varphi_1(k_1) & \cdots & \varphi_M(k_1) \\ & 1 & & \varphi_1(k_2) & \cdots & \varphi_M(k_2) \\ & & \ddots & \vdots & & \vdots \\ & & & 1 & \varphi_1(k_{N-M}) & \cdots & \varphi_M(k_{N-M}) \\ 0 & & & \varphi_1(k_1^c) & \cdots & \varphi_M(k_1^c) \\ & 0 & & \varphi_1(k_2^c) & \cdots & \varphi_M(k_2^c) \\ & & \ddots & \vdots & & \vdots \\ & & & 0 & \varphi_1(k_M^c) & \cdots & \varphi_M(k_M^c) \end{pmatrix} \\ &= \text{sgn}(K) \det \begin{pmatrix} \mathbb{1}_{N-M} & B(K, [M]) \\ O_M & B(K^c, [M]) \end{pmatrix}, \end{aligned} \quad (\text{B19})$$

where O_M is the $M \times M$ zero matrix. The $\text{sgn}(K)$ arises from the rearrangement of the rows. Thus one obtains

$$\begin{aligned} \det T([N]; K \cup \{N + 1, \dots, N + M\}) &= \text{sgn}(K) \det \mathbb{1}_{N-M} \det B(K^c; [M]) \\ &= \text{sgn}(K) \det B(K^c; [M]). \end{aligned} \quad (\text{B21})$$

Substituting Eq. (B21) into Eq. (B16) leads to

$$\begin{aligned} & \sum_{\sigma \in \mathcal{S}_N} \text{sgn}(\sigma) \varphi_1(x_{\sigma(1)}) \cdots \varphi_M(x_{\sigma(M)}) Z(x_{\sigma(M+1)}, x_{\sigma(M+2)}) \cdots \\ & \times Z(x_{\sigma(N-1)}, x_{\sigma(N)}) \end{aligned}$$

$$\begin{aligned} & \propto \sum_{K \in \binom{[N]}{N-M}} \text{pf} \mathcal{Z}(K; K) \\ & \times \det T([N]; K \cup \{N + 1, \dots, N + M\}). \end{aligned} \quad (\text{B22})$$

Now the wave function takes the form of a sum of products of a Pfaffian and a determinant. It follows from the theorem in Refs. [47,48] that

$$\begin{aligned} & \sum_{K \in \binom{[N]}{N-M}} \text{pf} \mathcal{Z}(K; K) \det T([N]; K \cup \{N + 1, \dots, N + M\}) \\ & = (-1)^{M(M-1)/2} \text{pf} \begin{pmatrix} GZG^T & H \\ -H^T & O_M \end{pmatrix}, \end{aligned} \quad (\text{B23})$$

where $G = T([N]; \{1, \dots, N\})$ and $H = T([N]; \{N + 1, \dots, N + M\})$.

In the present case, $G = \mathbb{1}_N$ and $H = B$, and thus one finally obtains

$$\langle x_1, \dots, x_N | \Psi \rangle \propto (-1)^{M(M-1)/2} \text{pf} \begin{pmatrix} \mathcal{Z} & B \\ -B^T & O_M \end{pmatrix}. \quad (\text{B24})$$

As mentioned earlier, this formula is valid also when $M =$ odd and $N - M =$ even [47]. Therefore it is applicable to an odd nuclei in which there is a blocked level. Notice that, in the HF case where $N = M$, Eq. (B24) reduces to the Slater

determinant [45,47,48]:

$$\begin{aligned} \Psi(x_1, x_2, \dots, x_N) &\propto (-1)^{M(M-1)/2} \text{pf} \begin{pmatrix} O_N & B \\ -B^T & O_N \end{pmatrix} \\ &= \det B. \end{aligned} \quad (\text{B25})$$

Therefore, Eq. (B24) for the BCS-type wave functions includes the Slater determinant for the HF case as a special case.

-
- [1] W Vonoertzen, M. Freer, and Yoshiko Kanada-En'yo, Nuclear clusters and nuclear molecules, *Phys. Rep.* **432**, 43 (2006).
- [2] *Clusters in Nuclei Volume 1*, edited by C. Beck, Lecture Notes in Physics Volume 818 (Springer, Berlin, 2010).
- [3] *Clusters in Nuclei Volume 2*, edited by C. Beck, Lecture Notes in Physics Volume 848 (Springer, Berlin, 2012).
- [4] J. Zhang, W. D. M. Rae, and A. C. Merchant, Systematics of some 3-dimensional α -cluster configurations in $4N$ nuclei from ^{16}O to ^{44}Ti , *Nucl. Phys. A* **575**, 61 (1994).
- [5] M. Freer, H. Horiuchi, Y. Kanada-En'yo, D. Lee, and Ulf-G. Meißner, Microscopic clustering in light nuclei, *Rev. Mod. Phys.* **90**, 035004 (2018).
- [6] M. Girod and P. Schuck, α -Particle Clustering from Expanding Self-Conjugate Nuclei within the Hartree-Fock-Bogoliubov Approach, *Phys. Rev. Lett.* **111**, 132503 (2013).
- [7] J.-P. Ebran, E. Khan, T. Nikšić, and D. Vretenar, Density functional theory studies of cluster states in nuclei, *Phys. Rev. C* **90**, 054329 (2014).
- [8] Y. Kanada-En'yo, M. Kimura, and A. Ono, Antisymmetrized molecular dynamics and its applications to cluster phenomena, *Prog. Theor. Exp. Phys.* **2012**, 01A202 (2012).
- [9] P.-G. Reinhard, J. A. Maruhn, A. S. Umar, and V. E. Oberacker, Localization in light nuclei, *Phys. Rev. C* **83**, 034312 (2011).
- [10] C. L. Zhang, B. Schuetrumpf, and W. Nazarewicz, Nucleon localization and fragment formation in nuclear fission, *Phys. Rev. C* **94**, 064323 (2016).
- [11] B. Schuetrumpf and W. Nazarewicz, Cluster formation in precompound nuclei in the time-dependent framework, *Phys. Rev. C* **96**, 064608 (2017).
- [12] J.-P. Ebran, E. Khan, and T. Nikšić, Localization and clustering in atomic nuclei, *J. Phys. G: Nucl. Part. Phys.* **44**, 103001 (2017).
- [13] Y. Tanimura, Clusterization and deformation of multi- Λ hypernuclei within a relativistic mean-field model, *Phys. Rev. C* **99**, 034324 (2019).
- [14] Z. X. Ren, D. Vretenar, T. Nikšić, P. W. Zhao, J. Zhao, and J. Meng, Dynamical Synthesis of ^4He in the Scission Phase of Nuclear Fission, *Phys. Rev. Lett.* **128**, 172501 (2022).
- [15] J. A. Maruhn, M. Kimura, S. Schramm, P.-G. Reinhard, H. Horiuchi, and A. Tohsaki, α -cluster structure and exotic states in a self-consistent model for light nuclei, *Phys. Rev. C* **74**, 044311 (2006).
- [16] H. Horiuchi, Chapter III. Kernels of GCM, RGM and OCM and their calculation methods, *Prog. Theor. Phys. Suppl.* **62**, 90 (1977).
- [17] M. Kimura and H. Horiuchi, Coexistence of cluster structure and superdeformation in ^{44}Ti , *Nucl. Phys. A* **767**, 58 (2006).
- [18] Y. Kanada-En'yo, T. Suhara, and Y. Taniguchi, Approximation of reduced width amplitude and application to cluster decay width, *Prog. Theor. Exp. Phys.* **2014**, 073D02 (2014).
- [19] Y. Taniguchi, K. Yoshida, Y. Chiba, Y. Kanada-En'yo, M. Kimura, and K. Ogata, Unexpectedly enhanced α -particle preformation in ^{48}Ti probed by the $(p, p'\alpha)$ reaction, *Phys. Rev. C* **103**, L031305 (2021).
- [20] Y. Liu, T. J. Frankcombe, and T. W. Schmidt, Chemical bonding motifs from a tiling of the many-electron wavefunction, *Phys. Chem. Chem. Phys.* **18**, 13385 (2016), and the references therein.
- [21] Y. Liu, P. Kilby, T. J. Frankcombe, and T. W. Schmidt, The electronic structure of benzene from a tiling of the correlated 126-dimensional wavefunction, *Nat. Commun.* **11**, 1210 (2020).
- [22] Y. Liu, T. J. Frankcombe, and T. W. Schmidt, Visualizing the 30-dimensional antisymmetrized electronic structure of water: The emergence of lone pairs, *J. Phys. Chem. Lett.* **11**, 735 (2020).
- [23] Y. Liu, P. Kilby, T. J. Frankcombe, and T. W. Schmidt, Electronic transitions of molecules: Vibrating Lewis structures, *Chem. Sci.* **10**, 6809 (2019).
- [24] M. V. Zhukov, A. A. Korshennikov, and M. H. Smedberg, Simplified $\alpha + 4n$ model for the ^8He nucleus, *Phys. Rev. C* **50**, R1(R) (1994).
- [25] K. Hagino and H. Sagawa, Pairing correlations in nuclei on the neutron-drip line, *Phys. Rev. C* **72**, 044321 (2005).
- [26] K. Hagino, H. Sagawa, J. Carbonell, and P. Schuck, Coexistence of BCS- and BEC-Like Pair Structures in Halo Nuclei, *Phys. Rev. Lett.* **99**, 022506 (2007).
- [27] E. Hiyama, R. Lazauskas, F. M. Marqués, and J. Carbonell, Modeling ^{19}B as a ^{17}B - n - n three-body system in the unitary limit, *Phys. Rev. C* **100**, 011603(R) (2019).
- [28] A. Ono, H. Horiuchi, T. Maruyama, and A. Ohnishi, Antisymmetrized version of molecular dynamics with two-nucleon collisions and its application to heavy ion reactions, *Prog. Theor. Phys.* **87**, 1185 (1992).
- [29] E. Chabanat, P. Bonche, P. Haensel, J. Meyer, and R. Schaeffer, A Skyrme parametrization from subnuclear to neutron star densities Part II. Nuclei far from stabilities, *Nucl. Phys. A* **635**, 231 (1998).
- [30] D. Vautherin, Hartree-Fock calculations with Skyrme's interaction. II. Axially deformed nuclei, *Phys. Rev. C* **7**, 296 (1973).
- [31] W. H. Press, S. A. Teukolsky, W. T. Vetterling, and B. P. Flannery, *Numerical Recipes in Fortran 77* (Cambridge University Press, Cambridge, 1986).
- [32] P. Ring and P. Schuck, *The Nuclear Many-body Problems* (Springer, Berlin, 1980).

- [33] A. D. Becke and K. E. Edgecombe, A simple measure of electron localization in atomic and molecular systems, *J. Chem. Phys.* **92**, 5397 (1990).
- [34] P. Jerabek, B. Schuetrumpf, P. Schwerdtfeger, and W. Nazarewicz, Electron and Nucleon Localization Functions of Oganesson: Approaching the Thomas-Fermi Limit, *Phys. Rev. Lett.* **120**, 053001 (2018).
- [35] A. S. Umar, C. Simenel, and K. Godbey, Pauli energy contribution to the nucleus-nucleus interaction, *Phys. Rev. C* **104**, 034619 (2021).
- [36] See Supplemental Material at <http://link.aps.org/supplemental/10.1103/PhysRevC.106.014307> for the animated views of Figs. 2–6, and for the evolution of neutron configuration shown in Fig. 10 as the deformation increases.
- [37] E. Perlińska, S. G. Rohoziński, J. Dobaczewski, and W. Nazarewicz, Local density approximation for proton-neutron pairing correlations: Formalism, *Phys. Rev. C* **69**, 014316 (2004).
- [38] K. Sato, J. Dobaczewski, T. Nakatsukasa, and W. Satuła, Energy-density-functional calculations including proton-neutron mixing, *Phys. Rev. C* **88**, 061301(R) (2013).
- [39] J. A. Sheikh, N. Hinohara, J. Dobaczewski, T. Nakatsukasa, W. Nazarewicz, and K. Sato, Isospin-invariant Skyrme energy-density-functional approach with axial symmetry, *Phys. Rev. C* **89**, 054317 (2014).
- [40] S. Frauendorf and A. O. Macchiavelli, Overview of neutron-proton pairing, *Prog. Part. Nucl. Phys.* **78**, 24 (2014).
- [41] R. Bijker and F. Iachello, Cluster structure of ^{20}Ne : Evidence for \mathcal{D}_{3h} symmetry, *Nucl. Phys. A* **1006**, 122077 (2021).
- [42] D. J. Rowe, *Nuclear Collective Motion—Models and Theory* (World Scientific, Singapore, 2010).
- [43] J. P. Bouchaud, A. Georges, and C. Lhuillier, Pair wave functions for strongly correlated fermions and their determinantal representation, *J. Phys. France* **49**, 553 (1988).
- [44] M. Bajdich, L. Mitas, G. Drobný, L. K. Wagner, and K. E. Schmidt, Pfaffian Pairing Wave Functions in Electronic-Structure Quantum Monte Carlo Simulations, *Phys. Rev. Lett.* **96**, 130201 (2006).
- [45] M. Bajdich, L. Mitas, L. K. Wagner, and K. E. Schmidt, Pfaffian pairing and backflow wave functions for electronic structure quantum Monte Carlo methods, *Phys. Rev. B* **77**, 115112 (2008).
- [46] C. Genovese, T. Shirakawa, K. Nakano, and S. Sorella, General correlated geminal ansatz for electronic structure calculations: Exploiting Pfaffians in Place of Determinants, *J. Chem. Theory Comput.* **16**, 6114 (2020).
- [47] M. Ishikawa and M. Wakayama, Minor summation formula of pfaffians, *Linear Multilinear Algebra* **39**, 285 (1995).
- [48] S. Okada, Pfaffian formula and Schur Q -function identities, *Adv. Math* **353**, 446 (2019).